DOI 10.24425/aee.2024.149919

High frequency oscillation analysis and suppression strategy of flexible direct current system

FANG ZHANG ✉, XIUGONG LIANG, WENPENG YAO

School of Electrical and Information Engineering, Tianjin University
92 Weijin RoadNankai District, Tianjin, China
e-mail: {✉ zhangfang/2021234021}@tju.edu.cn, 253329561@qq.com

(Received: 04.07.2023, revised: 18.04.2024)

Abstract: In recent years, the high frequency oscillation (HFO) accidents caused by long link delay in modular multilevel converter-based high-voltage direct current (MMC-HVDC) transmission projects have posed new challenges to the safety and stability of power system operation. This paper adopts delay stability margin to measure the high frequency stability of the MMC-HVDC system and derives the state space model of the MMC-HVDC time-delay system considering the link delay. The Lyapunov direct method is extended to the stability analysis of the MMC-HVDC time-delay system and the delay stability margin of the system is solved based on the linear matrix inequality (LMI). Then the influence of the controller parameters on the delay stability margin of the MMC-HVDC system is analyzed. Based on improved Smith predictive compensation control, an HFO suppression strategy of the MMC-HVDC system is proposed to improve the high frequency stability of the system by equivalently reducing and eliminating the total link delay. The effectiveness of the Lyapunov direct method for solving the delay stability margin of the MMC-HVDC system and the superiority of the proposed HFO suppression strategy are verified by the time-domain simulation in PSCAD/EMTDC. The research provides a novel viewpoint for the study of the HFO and suppression strategy of the MMC-HVDC system.

Key words: delay stability margin, HFO, improved Smith predictive compensation control, Lyapunov direct method, MMC-HVDC

1. Introduction

The rapid development of high voltage direct current (HVDC) based on modular multi-level converters (MMCs) has been driven by their suitability for large-scale integration of renewable energy sources [1]. However, this progress has brought about an increase in the occurrence of high

frequency oscillation (HFO). Several HFO events of different types have been reported worldwide. For instance, a 290 Hz oscillation event occurred in BorWin1 of Germany [2] and the 1.6 kHz oscillation in the INELFE France-Spain grid interconnection project [3]. Similarly, the 1 270 Hz oscillation in the Lu'Xi HVDC project [4], the 700 Hz/1 800 Hz oscillations in the Yu'E HVDC project [5] and the 2 kHz oscillation in the Rudong MMC-HVDC-based offshore wind farm integration project occurred in China [6]. HFO not only degrades the energy transmission efficiency of the MMC station but also deteriorates its power quality. In severe cases, they can lead to the converter station to trip, which poses a great threat to the safe and stable operation of the power system [7]. Therefore, analyzing the mechanism of HFO and designing oscillation suppression strategies have important theoretical significance and practiced value to ensure the safe and stable operation of the MMC-HVDC system.

Currently, there are two main methods for analyzing the mechanism of HFO: impedance analysis and eigenvalue analysis methods. The impedance analysis method takes port current and voltage as input and output to obtain an impedance model and base on which the frequency response characteristics of the system are analyzed. The stability of the system is analyzed through Bode plots or Nyquist curves [8]. Without considering the sub-module (SM) capacitor voltage dynamics, the impedance of MMC is a multi-input multi-output (MIMO) transfer function, which requires the use of generalized the Nyquist theory to analyze the stability of the system [9]. When the system is analyzed using sequence impedance, the high-frequency responses of positive and negative sequence impedances are almost identical. At this time, the MMC can be considered as a single-input single-output (SISO) system, and the positive sequence impedance is used as the transfer function of the system [10]. However, when using the impedance analysis method, the conclusion obtained is the stability of the port, so it cannot reflect the internal stability of the MMC [11].

The eigenvalue analysis method determines the stability of a system by solving for the eigenvalues of the Jacobian matrix of the system. If all the real parts of the eigenvalues are negative, the system is stable, otherwise, it is unstable. With the in-depth research on the MMC-HVDC system by the eigenvalue analysis method, the effects of the phase-locked loop (PLL), outer and inner loops, circulating current suppression controller (CCSC), and AC grid strength on HFO are gradually revealed. Among them, the inner loop current controller has a significant influence on the HFO of the system [12]. Due to the inclusion of time delay in the modulation section, i.e., e^{-sTd}, Td represents time delay, the characteristic equations become transcendental equations, which makes it impossible to directly solve the eigenvalues. In [13], the link delay in the MMC-HVDC system is replaced by the Pade approximation, and the transcendental equations are transformed into rational characteristic equations. It is found that the link delay has a significant impact on the high-frequency stability of the system. However, the Pade approximation introduces additional differential state equations, increasing the complexity of the model. Moreover, if various delays in the system are taken into account, the order of the state equations will become very high, leading to a "disaster of dimensionality" [14].

Based on the above research, it is known that the MMC-HVDC system can be regarded as a nonlinear time-delay system. As far as current research is concerned, the Lyapunov direct method is widely used in the stability studies of time-delay power systems [15]. However, no scholars have yet extended the Lyapunov direct method to the study of the stability of the MMC-HVDC time-delay system.

As far as the suppression strategy of HFO is concerned, the embedded filter method and the damping method are mainly used for the MMC-HVDC system. A low-pass filter is embedded in the grid voltage feedforward path of the current inner loop control to improve the phase margin of the system in the high frequency band and suppress the HFO of the system [4]. In [16], the third-order filter and the second-order filter are inserted into the voltage feedforward path and the proportional path of the current controller, respectively, and it is concluded that the lower bandwidth and higher order are more beneficial to the suppression of HFO. Two suppression strategies are proposed in [5]: one is to replace the low-pass filter of the voltage feedforward path with a round function and the other is to design a second-order damping controller to imitate the passive filter. Both methods can effectively suppress the HFO of the MMC-HVDC system. However, the methods of embedded filters in the grid voltage feedforward path used in [16] and the damping method used in [5] have not fundamentally eliminated the effect of delay on the deterioration of the system stability. In addition, [17] and [18] provide a robust control strategy based on H_2/H_∞, which are applied to the suppressions of low frequency and high frequency oscillations, respectively, but the controller has more parameters and the design is more complex. The Smith predictive compensation control algorithm is proposed for the first time in [19], which predicts the dynamic response of the system in advance and equivalently compensates the time delay of the system by adding the Smith predictive compensation to the feedback channel. So far, the Smith predictive compensation control has been applied to temperature control systems [20], network control systems [21], and photoelectric tracking systems [22], which effectively overcome the influence of the time delay on the system stability. However, there is no literature to apply the Smith predictive compensation control to suppress HFO of the MMC-HVDC system.

The remainder of this paper is organized as follows. Section 2 introduces the MMC-HVDC system. In Section 3, the state space model of the MMC-HVDC time-delay system is established and the stability analysis method is proposed. In Section 4, the influence factors of high-frequency stability for the MMC-HVDC time-delay system are analyzed. Section 5 proposes a suppression strategy of HFO for the MMC-HVDC system based on improved Smith predictive compensation control. Simulation results are presented and discussed in Section 6. The conclusions are drawn in Section 7.

2. Study system

The main circuit and control structure of the MMC-HVDC system are depicted in Fig. 1, in which the MMC adopts the double closed-loop PI control based on rotating the dq frame and the CSCC adopts PI control. In the actual HVDC project, the total link delay of the MMC-HVDC system includes electrical quantity sampling, pole control, valve control, modulation and SM switching [9]. As shown in Fig. 1, the total link delay of the MMC-HVDC system is denoted by G_d, where $G_\mathrm{d} = e^{-\tau s}$, τ represents the total system link delay.

The single-phase topology of the MMC is shown in Fig. 2. U_dc and I_dc denote DC voltage and current, respectively. L_a and R_a represent the arm inductance and resistance, respectively. u_i, i_i and m_i $(i = P, N)$ represent the MMC upper and lower arm voltage, current and switching function, respectively. u_f and i_c are the converter AC side voltage and current, respectively. i_cir represents the arm circulating current, which mainly contains DC and a second harmonic component. L_s and R_s

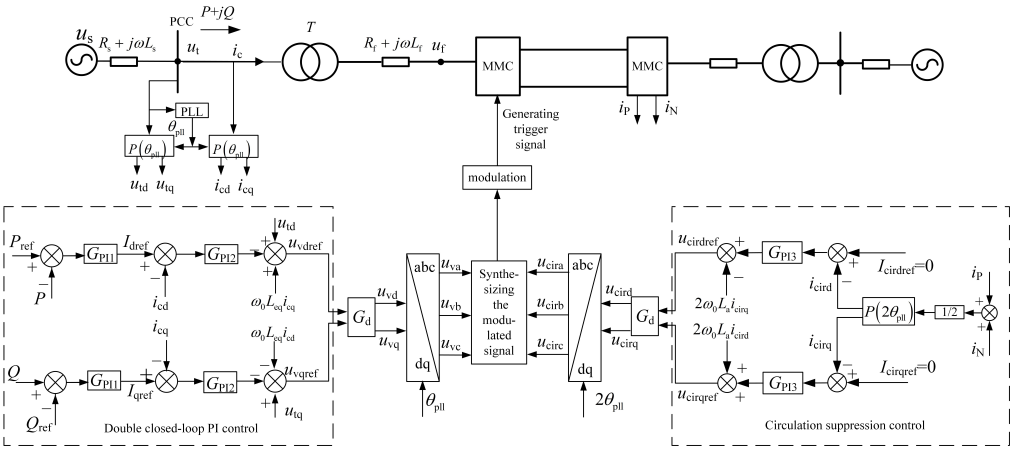

Fig. 1. Model and control block diagram of MMC-HVDC system

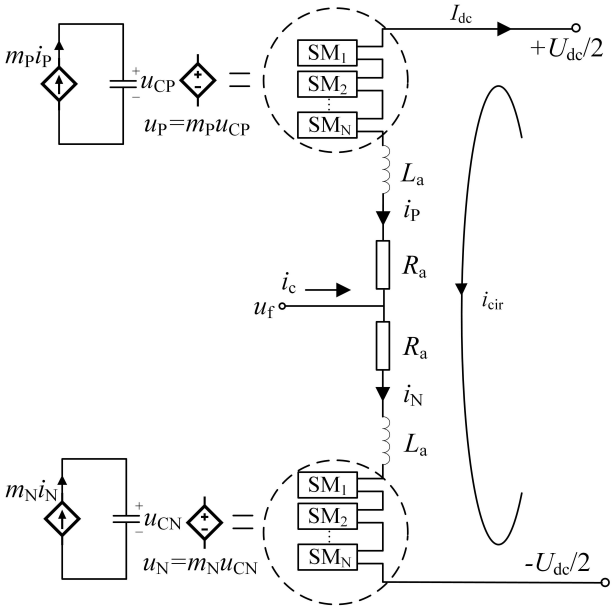

Fig. 2. Single phase topology of MMC

represent the inductance and resistance of the AC grid, respectively. The equivalent mathematical model of the MMC-HVDC system is $G(s) = 1/(sL_{eq} + R_{eq})$, where $R_{eq} = R_T + R_f + R_a/2$ and $L_{eq} = L_T + L_f + L_a/2$, L_T and R_T denote the transformer equivalent inductance and resistance, respectively. L_f and R_f are the phase reactor inductance and resistance, respectively. This paper focuses on the HFO between the rectifier-side MMC and the AC system. Therefore, assumed that the inverter-side MMC maintains the DC voltage constant through DC voltage control.

3. System modeling and stability analysis method

3.1. State space model of MMC-HVDC time-delay system

According to existing research and engineering cases, the bandwidth of power outer-loop control of the MMC-HVDC system is far less than that of current inner-loop control. As a result, the influence of the outer-loop control on HFO can be ignored [4, 9]. In this section, a state-space model of the MMC-HVDC time-delay system considering the SM capacitor voltage dynamics, current inner loop control, PLL and CCSC is developed, as shown in Appendix A.

Through eliminating the algebraic variables of differential equations, the time-delay differential equations containing only state variables are obtained as

$$\dot{\boldsymbol{x}} = f\left(x, x\left(t-\tau\right)\right), \tag{1}$$

where $\boldsymbol{x}$ and $\boldsymbol{x}\left(t-\tau\right)$ represent the state variables without time delay and ones with time delay of the MMC-HVDC system, respectively.

Linearizing Eq. (1) at the equilibrium point to obtain the small signal differential equations as follows:

$$\Delta\dot{\boldsymbol{x}} = \boldsymbol{A}_0\Delta\boldsymbol{x} + \boldsymbol{A}_\tau\Delta\boldsymbol{x}\left(t-\tau\right), \tag{2}$$

where $\boldsymbol{A}_0$ and $\boldsymbol{A}_\tau$ represent the Jacobi matrix composed of state variables without time delay and ones with time delay, respectively.

3.2. Lyapunov stability criterion based on LMI

The theory of linear matrix inequality (LMI) has led to the widespread use of the Lyapunov–Krasovskii direct method as the main method for studying the stability of time-delay systems [23]. Therefore, this paper combines the Lyapunov–Krasovskii theorem and LMI to analyze the high frequency stability of the MMC-HVDC time-delay system.

The Lyapunov–Krasovskii theorem is briefly stated as follows: Firstly, establish a bounded positive definite Lyapunov function $\boldsymbol{V}$. If the derivative of the function $\boldsymbol{V}$ along the trajectory of the time-delay dynamical system is negative definite, the time-delay system can be determined to be asymptotically stable. Based on methods of model transformation, the problem of a negative definite derivative function can be transformed into the problem of solving linear matrix inequality [23].

For the small signal MMC-HVDC time-delay system shown in Eq. (2), the LMI form of the Lyapunov stability criterion is briefly stated as follows: given a scalar $h > 0$, if exist $\boldsymbol{X}_{11} = \boldsymbol{X}_{12}^T > 0$, $\boldsymbol{X}_{22} = \boldsymbol{X}_{22}^T > 0$, $\boldsymbol{P} = \boldsymbol{P}^T > 0$, $\boldsymbol{Q} = \boldsymbol{Q}^T > 0$, $\boldsymbol{Z} = \boldsymbol{Z}^T > 0$ and matrices $\boldsymbol{N}_1$, $\boldsymbol{N}_2$, $\boldsymbol{X}_{12}$ with suitable dimension so that inequalities (3) and (4) hold, the time-delay system expressed as Eq. (2) is asymptotically stable for all time delay $\tau \in [0, h]$ [24].

$$\boldsymbol{\Phi} = \begin{bmatrix} \boldsymbol{\Phi}_{11} + h\boldsymbol{A}_0^T\boldsymbol{Z}\boldsymbol{A}_0 & \boldsymbol{\Phi}_{12} + h\boldsymbol{A}_0^T\boldsymbol{Z}\boldsymbol{A}_\tau \\ \boldsymbol{\Phi}_{12}^T + h\boldsymbol{A}_\tau^T\boldsymbol{Z}\boldsymbol{A}_0 & \boldsymbol{\Phi}_{22} + h\boldsymbol{A}_\tau^T\boldsymbol{Z}\boldsymbol{A}_\tau \end{bmatrix} < 0, \tag{3}$$

$$\boldsymbol{\Psi} = \begin{bmatrix} \boldsymbol{X}_{11} & \boldsymbol{X}_{12} & \boldsymbol{N}_1 \\ \boldsymbol{X}_{12}^T & \boldsymbol{X}_{22} & \boldsymbol{N}_2 \\ \boldsymbol{N}_1^T & \boldsymbol{N}_2^T & \boldsymbol{Z} \end{bmatrix} > 0, \tag{4}$$

where

$$\begin{aligned}\boldsymbol{\Phi}_{11} &= \boldsymbol{P}\boldsymbol{A}_0 + \boldsymbol{A}_0^T\boldsymbol{P} + \boldsymbol{N}_1 + \boldsymbol{N}_1^T + \boldsymbol{Q} + h\boldsymbol{X}_{11},\\ \boldsymbol{\Phi}_{12} &= \boldsymbol{P}\boldsymbol{A}_\tau - \boldsymbol{N}_1 + \boldsymbol{N}_2^T + h\boldsymbol{X}_{12},\\ \boldsymbol{\Phi}_{22} &= -\boldsymbol{N}_2 - \boldsymbol{N}_2^T - \boldsymbol{Q} + h\boldsymbol{X}_{22}.\end{aligned}$$

3.3. Solving steps of delay stability margin for MMC-HVDC system

Based on the small-signal mathematical model of the MMC-HVDC time-delay system and the Lyapunov stability criterion, the delay stability margin of the MMC-HVDC system is solved as follows:

1. Time-delay differential equations as shown in Eq. (1) of the MMC-HVDC system are obtained by eliminating the algebraic variables, and through linearizing it at the equilibrium point of the system, the standard form is obtained as Eq. (2).
2. Give a large search interval $[\tau_{\min}, \tau_{\max}]$ containing the delay stability margin of the system and the time accuracy τ_{ac}.
3. Let $h = (\tau_{\min} + \tau_{\max})/2$ and establish the LMI in MATLAB as shown in inequalities (3) and (4) to transform the stability problem for the time-delay system into an LMI feasibility problem.
4. Use the feasp solver of the LMI toolbox in MATLAB to judge the feasibility of inequalities (3) and (4), i.e., whether the above two LMIs hold or not.
5. If the LMIs hold, let $\tau_{\min} = h$; conversely, let $\tau_{\max} = h$.
6. Judge whether $|\tau_{\max} - \tau_{\min}| < \tau_{\text{ac}}$ is true, if so, the delay stability margin of the system is h; otherwise, return to step 3 to repeat the process above until the upper limit h of the MMC-HVDC system with a given accuracy is obtained. h is named as delay stability margin.

It is known that the delay stability margin can measure the high frequency stability of the MMC-HVDC system [18]. In this paper, the delay stability margin of the MMC-HVDC system is solved by the Lyapunov direct method, which provides a new idea for the safety and stability assessment of MMC-HVDC projects.

4. Influence factors analysis of MMC-HVDC time-delay system

The electromagnetic transient simulation model of the MMC-HVDC system shown in Fig. 1 is established in the PSCAD/EMTDC platform. The model parameters and control parameters of the MMC-HVDC system are shown in Appendix B.

4.1. Influence of current inner loop parameters on delay stability margin

Changing the proportional coefficient of the current inner loop shown in Table B.2 in App. B with other parameters constant, let it increase from 4 to 7 with steps of 0.5. The same is true of the integral coefficient, increasing it from 125 to 185 with steps of 10. The delay stability margin of the MMC-HVDC system solved by the Lyapunov direct method is shown in Table 1.

According to Table 1, while the proportional coefficient of the current inner loop increases from 4 to 7, the delay stability margin of the MMC-HVDC system solved by the Lyapunov direct method significantly decreases from 396.35 μs to 232.47 μs, decreasing by 41.35%, and the risk of HFO caused by link delay also increases, which is consistent with the conclusion of

Table 1. Influence of current inner loop parameters on delay stability margin

Proportional coefficient	**Delay stability margin/ μs**	**Integral coefficient**	**Delay stability margin/ μs**
4.0	396.35	125	321.05
4.5	354.77	135	320.99
5.0	321.05	145	320.94
5.5	293.15	155	320.88
6.0	269.70	165	320.83
6.5	249.71	175	320.77
7.0	232.47	185	320.72

references [14, 18]. However, while the integral coefficient of the current inner loop increases from 125 to 185, the delay stability margin of the MMC-HVDC solved by the Lyapunov direct method slightly decreases from 321.05 μs to 320.72 μs, with the variation range of only 0.10%. Therefore, in the actual MMC-HVDC project, the proportional coefficient of the current inner loop should be selected as small as possible to ensure that the system has sufficient safety and stability margin and the influence of the integral coefficient of the current inner loop on the high-frequency stability of the MMC-HVDC system can be ignored.

4.2. Influence of PLL parameters on delay stability margin

The PLL provides the Park transform angle for the control system of the MMC-HVDC. Some scholars have mainly studied the influence of the PLL on the system's stability under the condition of a weak AC grid connection in [25]. Generally speaking, the MMC-HVDC is connected with a strong AC system. Thus, in order to fully explore the main factors affecting the time-delay stability of the MMC-HVDC system, this section investigates the influence of PLL control parameters on the delay stability margin of the MMC-HVDC system.

Changing the proportional coefficient of the PLL shown in Table B.2 in App. B with other parameters constant, let it increase from 10 to 70 with steps of 10. The same is true of the integral coefficient, increasing it from 100 to 160 with steps of 10. The delay stability margin of the MMC-HVDC system solved by the Lyapunov direct method is shown in Table 2.

Table 2. Influence of PLL parameters on delay stability margin

Proportional coefficient	**Delay stability margin/ μs**	**Integral coefficient**	**Delay stability margin/ μs**
10	320.97	100	321.05
20	320.99	110	321.05
30	321.01	120	321.05
40	321.03	130	321.05
50	321.05	140	321.05
60	321.07	150	321.05
70	321.09	160	321.05

According to Table 2, while the PLL proportional coefficient increases from 10 to 70 and the integral coefficient increases from 100 to 160, respectively, the delay stability margin of the MMC-HVDC system solved by the Lyapunov direct method is almost unchanged. In actual engineering, the PLL control parameters have almost no influence on the high-frequency stability of the MMC-HVDC system.

4.3. Influence of CCSC parameters on delay stability margin

The second harmonic current component with the negative-sequence property of the MMC circulates in the three-phase arm to form a circulating current. The circulating current causes distortion of the arm current, reduces the energy transfer efficiency of the MMC, and causes a certain degree of impact on the power devices. This section takes the circulation suppression strategy based on PI control as an example to study the influence of CCSC proportion and integral coefficients on the delay stability margin of the MMC-HVDC system.

Changing the CCSC proportional coefficient shown in Table B.2 in App. B with other parameters constant, let it increase from 0.2 to 1.4 with steps of 0.2. The same is true of the integral coefficient, increasing it from 10 to 70 with steps of 10. The delay stability margin of the MMC-HVDC system solved by the Lyapunov direct method is shown in Table 3.

Table 3. Influence of CCSC parameters on delay stability margin

Proportional coefficient	**Delay stability margin/ μs**	**Integral coefficient**	**Delay stability margin/ μs**
0.2	321.05	10	321.05
0.4	321.04	20	321.05
0.6	321.02	30	321.05
0.8	321.00	40	321.05
1.0	320.98	50	321.05
1.2	320.96	60	321.05
1.4	320.93	70	321.05

According to Table 3, while the CCSC proportional coefficient increases from 0.2 to 1.4 and the integral coefficient increases from 100 to 160, respectively, the delay stability margin of the MMC-HVDC system solved by the Lyapunov direct method is almost unchanged. In actual engineering, the CCSC parameters have almost no influence on the high frequency stability of the MMC-HVDC system.

4.4. Comparisons between the proposed method and the eigenvalue analysis method

To further state the effectiveness of the proposed method, this section makes comparisons between the conclusions of the Lyapunov direct method and the eigenvalue analysis method. To analyze the stability of HFO based on the eigenvalue analysis method, firstly the Pade approximation is applied to handle the delay term, G_{d}. The equations containing the delay term in the state space

model are replaced with rational polynomials, then linearized at the equilibrium point and the Jacobian matrix is calculated. Next, the eigenvalues of the Jacobian matrix are solved. Finally, the conclusions are compared and verified drawn with those based on the Lyapunov direct method.

4.4.1. The principle of Pade approximation

The Pade approximation is a method of using rational polynomials of order $[l, k]$ to approximate the delay of the transcendental term. The approximate method is as follows:

$$e^{-\tau_i s} \approx \frac{b_0 + b_1\tau_i s + \cdots + b_l\,(\tau_i s)^l}{a_0 + a_1\tau_i s + \cdots + a_k\,(\tau_i s)^k}, \tag{5}$$

where the coefficients a_j and b_j can be calculated by the Eq. (6).

$$a_j = \frac{(l+k-j)!k!}{j!\,(k-j)!}, \quad b_j = (-1)^j\,\frac{(l+k-j)!l!}{j!\,(l-j)!}. \tag{6}$$

This paper adopts the 4-order Pade approximation, i.e. $l = k = 4$.

4.4.2. Pade approximation for current inner loop control

Taking the d-axis as an example, the delay term, G_{d}, between the voltage reference value u_{vdref} obtained by the inner loop controller and the modulation point voltage u_{vd} as illustrated in Fig. 1 is replaced by the Pade approximation. The four additional differential equations and an algebraic equation after the Pade approximation are expressed as Eq. (7) and Eq. (8).

$$\begin{bmatrix} \dot{x}_{1\mathrm{d}} \\ \dot{x}_{2\mathrm{d}} \\ \dot{x}_{3\mathrm{d}} \\ \dot{x}_{4\mathrm{d}} \end{bmatrix} = \begin{bmatrix} 0 & 1 & 0 & 0 \\ 0 & 0 & 1 & 0 \\ 0 & 0 & 0 & 1 \\ -1680\tau^{-4} & -840\tau^{-3} & -180\tau^{-2} & -20\tau^{-1} \end{bmatrix} \begin{bmatrix} x_{1\mathrm{d}} \\ x_{2\mathrm{d}} \\ x_{3\mathrm{d}} \\ x_{4\mathrm{d}} \end{bmatrix} + \begin{bmatrix} 0 \\ 0 \\ 0 \\ 1 \end{bmatrix} \left(u_{\mathrm{td}} + \omega_0 L_{\mathrm{eq}} i_{\mathrm{cq}} - k_{\mathrm{pind}}(I_{\mathrm{dref}} - i_{\mathrm{cd}}) - k_{\mathrm{iind}} x_{\mathrm{ind}}\right), \tag{7}$$

$$u_{\mathrm{vd}} = -1680\tau^{-3} x_{2\mathrm{d}} - 40\tau^{-1} x_{4\mathrm{d}} + \left[u_{\mathrm{td}} + \omega_0 L_{\mathrm{eq}} i_{\mathrm{cq}} - k_{\mathrm{pind}}(I_{\mathrm{dref}} - i_{\mathrm{cd}}) - k_{\mathrm{iind}} x_{\mathrm{ind}}\right]. \tag{8}$$

The equations of the q-axis are the same. Due to space limitations, the equations will no longer be presented.

4.4.3. Result comparison

The mathematical model established in Section 3.1, which considers the SM capacitor voltage dynamics, current inner loop, phase-locked loop and CCSC, is appropriately simplified based on existing research conclusions. The research results in [5] indicate that the influence of the CCSC on HFO is minimal and can be ignored. In addition, this paper mainly studies the influence of controllers and the delay on HFO, so the capacitor voltage dynamics can be ignored in this section. The state space model used for the eigenvalue analysis method is a total of 14 orders, including 6-order non-time-delay state variables, $[i_{\mathrm{cd}}\ i_{\mathrm{cq}}\ x_{\mathrm{ind}}\ x_{\mathrm{inq}}\ x_{\mathrm{utq}}\ x_{\mathrm{pll}}]^T$ and 8-order state variables

introduced by the Pade approximation, $[x_{1d}\ x_{2d}\ x_{3d}\ x_{4d}\ x_{1q}\ x_{2q}\ x_{3q}\ x_{4q}]^T$, where x_{1q}, x_{2q}, x_{3q}, x_{4q} are state variables introduced by the q-axis Pade approximation for current inner loop control.

Figure 3(a) shows the root trajectory as the link delay is given, i.e. $\tau = 320$ μs, the proportional coefficient k_{pind} of the current inner loop increases from 5 to 5.5 with steps of 0.05, and other parameters remain constant. From Fig. 3(a), it can be seen that the proportional coefficient of the current inner loop, which makes the system critically stable, is about 5.15. The delay stability margin of the MMC-HVDC system is 321.05 μs by the Lyapunov direct method. According to Table 1 in Section 4.1, when $k_{\text{pind}} = 5$, the link delay, 320 μs, is less than the delay stability margin 321.05 μs, so the system is stable. When $k_{\text{pind}} = 5.5$, the link delay 320 μs is more than the delay stability margin 293.15 μs so the system is unstable. Therefore, the critically stable value of the proportional coefficient k_{pind} of the current inner loop is approximately between 5 and 5.5 by the Lyapunov direct method, which is basically consistent with the critically stable value of k_{pind}, 5.15, by the eigenvalue analysis method.

Figure 3(b) shows the root trajectory as the system link delay τ increases from 320 μs to 340 μs with steps of 2 μs, and other parameters remain constant. From Fig. 3(b), it can be seen that the link delay which makes the system critically stable is approximately 328 μs. Compared to Table 1 in Section 4.1, the delay stability margin of the MMC-HVDC system is 321.05 μs with $k_{\text{pind}} = 5$ by the Lyapunov direct method, which is basically consistent with the critically stable value of link delay τ, 328 μs, by the eigenvalue analysis method.

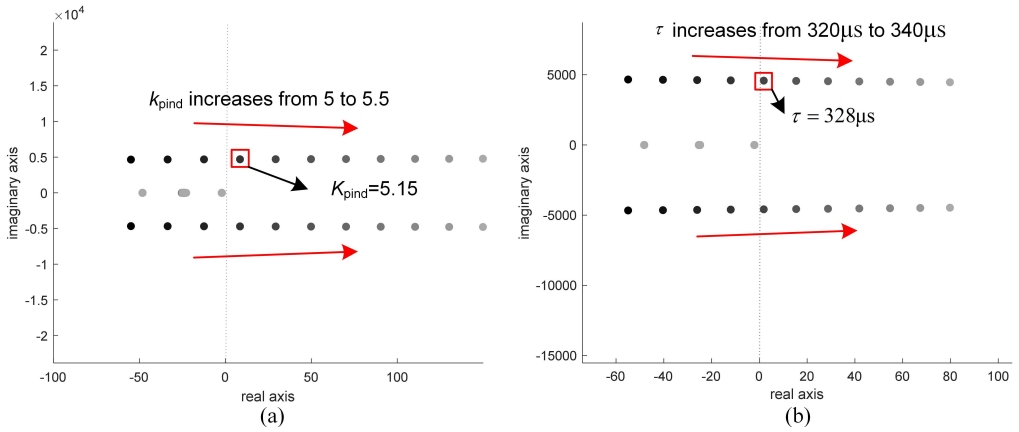

Fig. 3. Root trajectory diagram with parameters variation: (a) root trajectory diagram with the variation of the proportional coefficient k_{pind} of current inner loop; (b) root trajectory diagram with the variation of the link delay τ

To sum up, the conclusions of the proposed method and the eigenvalue analysis method are basically the same, however, the eigenvalue method cannot provide an indicator similar to the delay stability margin obtained by the Lyapunov method to judge the high-frequency stability of the system.

5. HFO suppression strategies of MMC-HVDC system

In this section, an improved Smith predictor is applied to the HFO suppression of the MMC-HVDC system, and an improved current inner loop control based on the improved Smith predictive compensation is proposed as shown in Fig. 4.

In Fig. 4, ω_2 represents the angular frequency of PLL output; $\hat{G}(s)$ and τ_{H} are the predictive model of the MMC-HVDC system and the predictive total link delay, respectively. $G_{\mathrm{f}} = 1/(1+T_{\mathrm{m}}s)$ is a first-order low-pass filter introduced to reduce the dependence of the Smith predictor on model parameters. When $G_{\mathrm{f}} = 1$, it degenerates into a traditional Smith predictor.

According to Fig. 4, the closed-loop transfer function from I_{dref} to i_{cd} can be obtained as

$$\frac{i_{\mathrm{cd}}}{I_{\mathrm{dref}}} = \frac{G_{\mathrm{PI1}} e^{-\tau s} G(s)}{1 + G_{\mathrm{PI1}} \hat{G}(s) + G_{\mathrm{f}} G_{\mathrm{PI1}} \left(G(s) e^{-\tau s} - \hat{G}(s) e^{-\tau_{\mathrm{H}} s} \right)}. \tag{9}$$

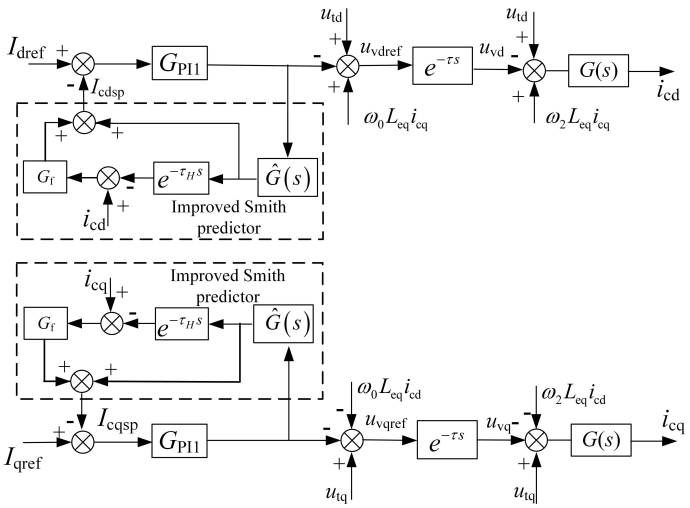

Fig. 4. Current inner loop control based on improved Smith predictive compensation

In Eq. (9), if the predictive model parameters and the predictive total link delay in the Smith predictor are consistent with the model parameters of the MMC-HVDC system and the total link delay, i.e. let $\hat{G}(s) = G(s)$, and $\tau_{\mathrm{H}} = \tau$, the system closed-loop transfer function can be simplified as

$$\frac{i_{\mathrm{cd}}}{I_{\mathrm{dref}}} = \frac{G_{\mathrm{PI1}} G(s)}{1 + G_{\mathrm{PI1}} G(s)} e^{-\tau s}. \tag{10}$$

From Eq. (10), it can be seen that the Smith predictive control makes the link delay move out of the closed-loop system so that the characteristic equation, i.e. the denominator of Eq. (10), no longer contains the delay term. The application of the Smith predictor can completely eliminate the effect of the link delay on the stability of the closed-loop transfer function and transform the time-delay system into a conventional constant system, which significantly improves the stability of the system.

However, if the predictive model parameters and the predictive total link delay of the Smith predictor do not match the actual model, the Smith predictor performance will be affected. Generally speaking, the model parameters of the MMC-HVDC system are known and basically not changed, i.e. $G(s) = 1/(sL_{\mathrm{eq}} + R_{\mathrm{eq}})$, where L_{eq} and R_{eq} are equivalent inductance and resistance mentioned in Section 2, so they remain unchanged. But the total link delay of the system, which is uncertain, needs to consider the influence of multiple processes such as sampling, valve control, communication and modulation, as well as the actual operating conditions.

To sum up, it may be assumed that the model parameters of the MMC-HVDC system in the Smith predictor can be predicted accurately, but the total link delay cannot be predicted accurately. The closed-loop transfer function expression for the d-axis current inner loop control based on the improved Smith prediction compensation can be simplified as

$$\frac{i_{\mathrm{cd}}}{I_{\mathrm{dref}}} = \frac{G_{\mathrm{PI1}} e^{-\tau s} G(s)}{1 + G_{\mathrm{PI1}} G(s) + G_{\mathrm{f}} G_{\mathrm{PI1}} G(s) (e^{-\tau s} - e^{-\tau_{\mathrm{H}} s})}. \tag{11}$$

According to Eq. (11), because of the inaccuracy of the Smith predictor for the total link delay prediction, the compensated characteristic equation, i.e. the denominator of Eq. (11), still contains the delay term, while the introduced low-pass filter G_{f} plays a certain buffering role in mismatched total link delay deviation and further improves the control performance of the Smith predictor.

6. Simulation verification

The electromagnetic transient simulation model of the MMC-HVDC system shown in Fig. 1 is built in the PSCAD/EMTDC simulation platform, and the system model parameters and control parameters are shown in Table B.1 and Table B.2 in App. B, respectively. In the simulation, the nearest level modulation (NLM) delay of a 41-level MMC-HVDC is about 165–175 μs. The NLM delay is taken as 170 μs below.

In this section, the time domain simulation verification will be carried out from the following aspects:

1. The feasibility and effectiveness of the Lyapunov direct method for solving the delay stability margin of the MMC-HVDC system.
2. The influence of the control parameters of the current inner loop on the high-frequency stability of the MMC-HVDC system.
3. The effectiveness and superiority of the HFO suppression strategy proposed in Section 5. The parameters of the PLL and CCSC basically do not influence the high-frequency stability of the system, which have been analyzed and verified in [5] and [18]. Due to the limited space, the influence of PLL and CCSC parameters on the high-frequency stability of the system are no longer verified by simulation in this paper.

6.1. Verification of the feasibility and validity of the Lyapunov direct method for solving the delay stability margin

With the given parameters in Table B.1 and Table B.2 in App. B, the delay stability margin of the MMC-HVDC system is 321.05 μs by solving the LMI shown in inequalities (3) and (4). If the total link delay of the MMC-HVDC system meets $\tau \in [0\ \mu\mathrm{s}, 321.05\ \mu\mathrm{s}]$, the MMC-HVDC system

can operate stably, else if the total link delay of the system is further increased, the LMI returns to an infeasible solution and the high frequency stability of the system cannot be guaranteed. In the electromagnetic transient simulation model of the MMC-HVDC system, set the system total link delay $\tau = 320$ μs. At $t = 1$ s, the total link delay increases to 350 μs, then at $t = 2$ s, the total link delay increases to 361 μs. The waveform of the d-axis current is illustrated in Fig. 5.

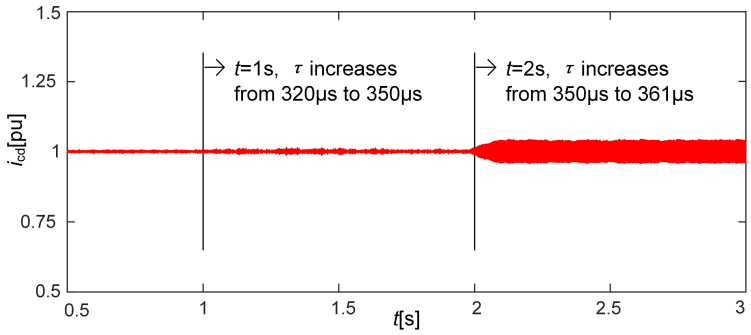

Fig. 5. The waveform of d-axis current with the increase of system total link delay

From Fig. 5, it can be seen that before 1 s, the MMC-HVDC system can operate stably because the total link delay of the MMC-HVDC system does not exceed the delay stability margin solved by the Lyapunov direct method. Because the Lyapunov direct method is conservative to some extent, when the total link delay increases to 350 μs, the system can still operate stably from 1 s to 2 s. When the total link delay further increases to 361 μs at $t = 2$ s, the waveform of the d-axis current is seriously distorted and the system cannot operate stably. Although the delay stability margin, 321.05 μs, solved by the Lyapunov direct method and that, 361 μs, obtained by the time-domain simulation method, have an error of 40 μs, the delay stability margin based on the Lyapunov direct method provides a new idea for analysis of high-frequency stability. The Fourier decomposition of the d-axis current from 2 s to 3 s and the harmonic components are revealed in Fig. 6.

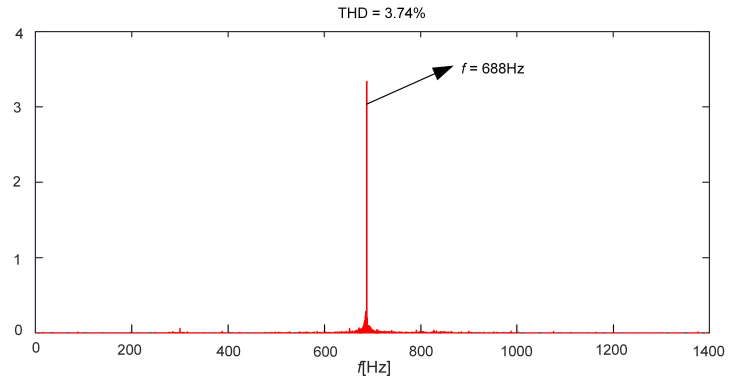

Fig. 6. Fourier decomposition results of d-axis current

From Fig. 6, it can be seen that the oscillation frequency of the d-axis current is 688 Hz, i.e., HFO occurs in the MMC-HVDC system. The feasibility and validity of the Lyapunov direct method to solve the delay stability margin of the MMC-HVDC system and to analyze the high-frequency stability of the system have been verified.

6.2. Verification of the influence of current inner loop control parameters on high frequency stability of MMC-HVDC

Set the total link delay $\tau = 337$ μs for the MMC-HVDC system. In order to verify the influence of the current inner loop control parameters on the high frequency stability of the MMC-HVDC system, two cases are set as follows.

Case 1: at $t = 1$ s, the dq-axis proportional coefficients of current inner loops k_{pind} and k_{pinq} increase from 5 to 5.5. The waveform of the d-axis current is depicted in Fig. 7(a).

Case 2: at $t = 1$ s, the dq-axis integral coefficients of current inner loops k_{iind} and k_{iinq} increase from 125 to 185. The waveform of the d-axis current is depicted in Fig. 7(b).

According to Fig. 7(a), it can be seen that before 1s, the waveform of the d-axis current is not distorted, and the MMC-HVDC system is in stable operation. At $t = 1$ s, the current inner-loop proportional coefficient increases from 5 to 5.5, and HFO occurs in the MMC-HVDC system. It is illustrated that increasing the current inner-loop proportional coefficient significantly reduces the delay stability margin of the MMC-HVDC system and deteriorates the high-frequency stability

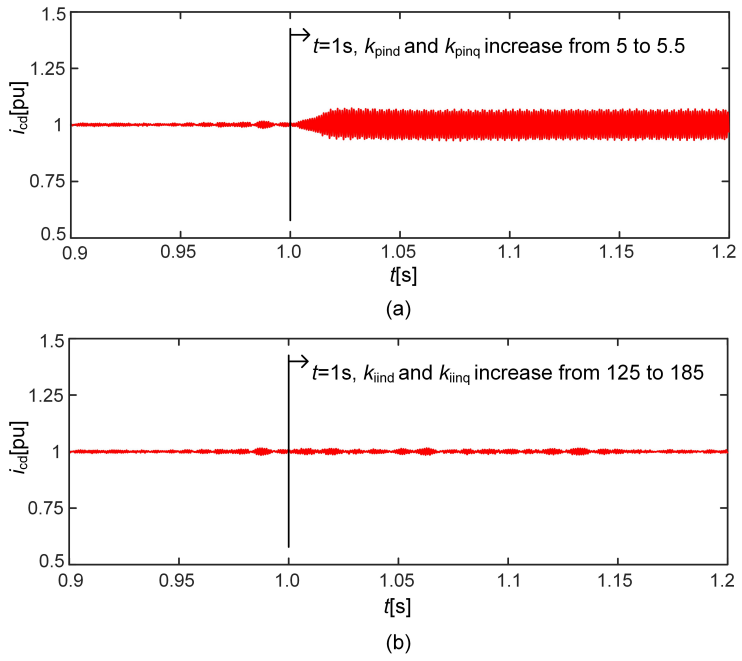

Fig. 7. The waveform of d-axis current with the variation of current inner loop controller parameters: (a) the waveform of d-axis current of Case 1; (b) the waveform of d-axis current of Case 2

of the system, which verifies the analysis results of the Lyapunov direct method in Section 4.1. Figure 7(b) reveals that the waveform of the d-axis current of the MMC-HVDC system is not distorted before and after the variation of the integral coefficient of the current inner loop, and the system is in stable operation. It is indicated that the integral coefficient of the current inner loop does not change the delay stability margin of the MMC-HVDC system and has no effect on the high-frequency stability basically, which verifies the analysis results of the Lyapunov direct method in Section 4.1.

6.3. Verify the effectiveness and superiority of HFO suppression strategy

6.3.1. Analysis of limitation of existing oscillation suppression strategy based on embedding filter

Embedding filters in the grid voltage feedforward loop is a common HFO suppression strategy for HVDC systems [4, 16]. The strategy is relatively simple, but the suppression effect is limited, as analyzed below in detail.

Case 3: set total link delay $\tau = 390$ μs for the MMC-HVDC system. At $t = 1$ s, a second-order low-pass filter with a cut-off frequency of 400 Hz is embedded into the grid voltage feedforward loop, and at $t = 2$ s, the proportional coefficient of the current inner loop increases from 5 to 6. The waveform of the d-axis current is shown in Fig. 8.

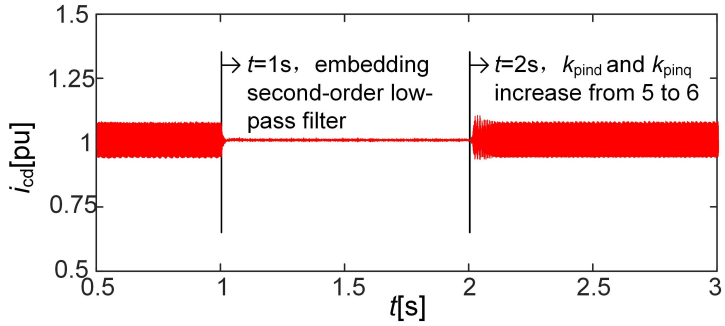

Fig. 8. The waveform of d-axis current based on filter oscillation suppression strategy

Figure 8 indicates that before 1 s, the MMC-HVDC system is in an HFO state with the long link delay $\tau = 390$ μs. At $t = 1$ s, a second-order low-pass filter is embedded into the grid voltage feedforward loop, by which the HFO of the MMC-HVDC system is effectively suppressed and the system quickly enters a stable operation. At $t = 2$ s, the proportional coefficient of the current inner loop increases from 5 to 6, the HFO occurs again. This case illustrates that the HFO suppression effect of the embedded filter into the grid voltage feedforward loop is limited, and it cannot deal with the sudden increase of the proportional coefficient of the current inner loop under certain circumstances.

6.3.2. Verification of HFO suppression strategy based on improved Smith predictive compensation control

To verify the effectiveness and superiority of the HFO suppression strategy based on the improved Smith predictive compensation control proposed in this paper, set the following case.

Case 4: set the total link delay of the system, the same as Case 3. At t = 1 s, the HFO suppression strategy based on the improved Smith predictive compensation control is put into operation, and at t = 2 s, the change of the proportional coefficient of the current inner loop is the same as Case 3. The waveform of the d-axis current based on the improved Smith predictive compensation control is shown in Fig. 9.

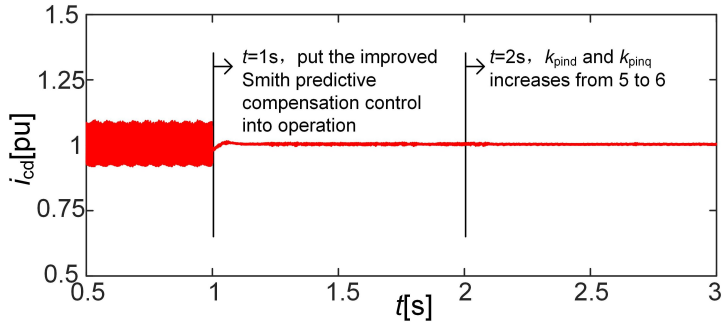

Fig. 9. The waveform of d-axis current based on improved Smith predictive compensation control

From Fig. 9, it can be seen that before 1 s, the MMC-HVDC system is in an HFO state with the long link delay τ = 390 μs. At t = 1 s, the HFO suppression strategy based on the improved Smith predictive compensation control is put into operation, the d-axis current reaches quickly the stable operation state from the HFO state, and the HFO of the MMC-HVDC system has been effectively suppressed, which verifies the effectiveness of the HFO suppression strategy based on the improved Smith predictive compensation control proposed in Section 5. At t = 2 s, the current inner loop proportional coefficient increases from 5 to 6, the waveform of the d-axis current is not distorted, and the system is still in the stable operation state. Compared with the simulation results of Case 3, the superiority of the HFO suppression strategy based on the improved Smith predictive compensation control proposed in Section 5 is verified.

7. Conclusions

In this paper, the state space model of the MMC-HVDC time-delay system is established and the high-frequency stability of the MMC-HVDC system is analysed by the Lyapunov direct method. From the perspective of compensating delay and offsetting delay, an HFO suppression strategy for the MMC-HVDC system based on an improved Smith predictive compensation control is proposed. The following conclusions are obtained.

1. The Lyapunov direct method does not need to deal with the delay term. The time-delay stability margin of the system can be obtained directly by solving LMI, which provides a new research idea for the high-frequency stability analysis of the MMC-HVDC time-delay system.
2. The delay stability margin is used to measure the high-frequency stability of the MMC-HVDC system. The proportional coefficient of the current inner loop has the most significant influence on the delay stability margin, and reducing the proportional coefficient of the

current inner loop can improve the high-frequency stability of the system. PLL and CCSC parameters have almost no influence on the high-frequency stability of the system. This method provides a theoretical basis for the selection of engineering parameters of the time-delay MMC-HVDC system.

3. An HFO suppression strategy based on an improved Smith predictive compensation control is proposed in this paper, which improves the high-frequency stability of the MMC-HVDC system by equivalently reducing the total link delay. This strategy can ensure that the system continues to operate stably after the proportional coefficient of the current inner loop increases, and the system can achieve better control performance than the existing HFO suppression strategies.

Appendix A

In this paper, a state-space model considering the MMC-HVDC time-delay system SM capacitor voltage dynamics, arm circulating current, current inner loop control, PLL and CCSC is given. The state equations of the MMC are shown in equations (A.1–A.8), where u_{cp0}, u_{cpd}, u_{cpq}, u_{cpd2}, u_{cpq2} are the DC, d-axis and q-axis fundamental frequency, d-axis and q-axis second harmonic components of the arm equivalent capacitor voltage, respectively; i_{cir0}, i_{cird}, i_{cirq} represent the DC, d-axis and q-axis second harmonic circulating current components of the arm current, respectively; i_{cd}, i_{cq} represent the d-axis and q-axis components of the AC system current flowing into the MMC-HVDC system, respectively; u_{vd}, u_{vq} represent the d-axis and q-axis components of the MMC modulation point voltage, respectively; u_{cird}, u_{cirq} represent the d-axis and q-axis amount of correction for modulation voltage from the CCSC; C_{eq} is the equivalent capacitance of the arm, where $C_{eq} = C/n$, n is the number of SMs.

$$C_{eq}\frac{du_{cp0}}{dt} = \frac{1}{2}i_{cir0} + \frac{1}{4}\frac{u_{vd}}{U_{dc}}i_{cd} + \frac{1}{4}\frac{u_{vq}}{U_{dc}}i_{cq} - \frac{1}{2}\frac{u_{cird}}{U_{dc}}i_{cird} - \frac{1}{2}\frac{u_{cirq}}{U_{dc}}i_{cirq}, \tag{A.1}$$

$$\begin{aligned} C_{eq}\frac{du_{cpd}}{dt} = {} & \omega_2 C_{eq}u_{cpq} - \frac{u_{vd}}{U_{dc}}i_{cir0} - \frac{1}{4}i_{cd} - \frac{1}{2}\frac{u_{vd}}{U_{dc}}i_{cird} \\ & - \frac{1}{2}\frac{u_{vq}}{U_{dc}}i_{cirq} + \frac{1}{4}\frac{u_{cird}}{U_{dc}}i_{cd} + \frac{1}{4}\frac{u_{cirq}}{U_{dc}}i_{cq}, \end{aligned} \tag{A.2}$$

$$\begin{aligned} C_{eq}\frac{du_{cpq}}{dt} = {} & -\omega_2 C_{eq}u_{cpd} - \frac{u_{vq}}{U_{dc}}i_{cir0} - \frac{1}{4}i_{cq} + \frac{1}{2}\frac{u_{vq}}{U_{dc}}i_{cird} \\ & - \frac{1}{2}\frac{u_{vd}}{U_{dc}}i_{cirq} - \frac{1}{4}\frac{u_{cird}}{U_{dc}}i_{cq} + \frac{1}{4}\frac{u_{cirq}}{U_{dc}}i_{cd}, \end{aligned} \tag{A.3}$$

$$C_{eq}\frac{du_{cpd2}}{dt} = 2\omega_2 C_{eq}u_{cpq2} + \frac{1}{4}\frac{u_{vd}}{U_{dc}}i_{cd} - \frac{1}{4}\frac{u_{vq}}{U_{dc}}i_{cq} + \frac{1}{2}i_{cird} - \frac{u_{cird}}{U_{dc}}i_{cir0}, \tag{A.4}$$

$$C_{eq}\frac{du_{cpq2}}{dt} = -2\omega_2 C_{eq}u_{cpd2} + \frac{1}{4}\frac{u_{vq}}{U_{dc}}i_{cd} + \frac{1}{4}\frac{u_{vd}}{U_{dc}}i_{cq} + \frac{1}{2}i_{cirq} - \frac{u_{cirq}}{U_{dc}}i_{cir0}, \tag{A.5}$$

$$\begin{aligned} L_a\frac{di_{cir0}}{dt} = {} & -R_a i_{cir0} + \frac{1}{2}U_{dc} - \frac{1}{2}u_{CP0} + \frac{1}{2}\frac{u_{vd}}{U_{dc}}u_{cpd} \\ & + \frac{1}{2}\frac{u_{vq}}{U_{dc}}u_{cpq} + \frac{1}{2}\frac{u_{cird}}{U_{dc}}u_{cpd2} + \frac{1}{2}\frac{u_{cirq}}{U_{dc}}u_{cpq2}, \end{aligned} \tag{A.6}$$

$$L_{\mathrm{a}}\frac{\mathrm{d}i_{\mathrm{cird}}}{\mathrm{d}t}=2\omega_2 L_{\mathrm{a}}i_{\mathrm{cirq}}-R_{\mathrm{a}}i_{\mathrm{cird}}+\frac{1}{2}\frac{u_{\mathrm{vd}}}{U_{\mathrm{dc}}}u_{\mathrm{cpd}}-\frac{1}{2}\frac{u_{\mathrm{vq}}}{U_{\mathrm{dc}}}u_{\mathrm{cpq}}+\frac{u_{\mathrm{cird}}}{U_{\mathrm{dc}}}u_{\mathrm{cp0}}-\frac{1}{2}u_{\mathrm{cpd2}}, \tag{A.7}$$

$$L_{\mathrm{a}}\frac{\mathrm{d}i_{\mathrm{cirq}}}{\mathrm{d}t}=-2\omega_2 L_{\mathrm{a}}i_{\mathrm{cird}}-R_{\mathrm{a}}i_{\mathrm{cirq}}+\frac{1}{2}\frac{u_{\mathrm{vq}}}{U_{\mathrm{dc}}}u_{\mathrm{cpd}}+\frac{1}{2}\frac{u_{\mathrm{vd}}}{U_{\mathrm{dc}}}u_{\mathrm{cpq}}+\frac{u_{\mathrm{cirq}}}{U_{\mathrm{dc}}}u_{\mathrm{cp0}}-\frac{1}{2}u_{\mathrm{cpq2}}. \tag{A.8}$$

The differential equations of equivalent inductance for the MMC-HVDC are:

$$\begin{cases} L_{\mathrm{eq}}\dfrac{\mathrm{d}i_{\mathrm{cd}}}{\mathrm{d}t}=U_{\mathrm{td}}-R_{\mathrm{eq}}i_{\mathrm{cd}}+\omega_2 L_{\mathrm{eq}}i_{\mathrm{cq}}-\dfrac{u_{\mathrm{vd}}}{U_{\mathrm{dc}}}u_{\mathrm{cp0}}+\dfrac{1}{2}u_{\mathrm{cpd}}-\dfrac{1}{2}\dfrac{u_{\mathrm{cird}}}{U_{\mathrm{dc}}}u_{\mathrm{cpd}} \\ \qquad\qquad -\dfrac{1}{2}\dfrac{u_{\mathrm{cirq}}}{U_{\mathrm{dc}}}u_{\mathrm{cpq}}-\dfrac{1}{2}u_{\mathrm{cpd2}}\dfrac{u_{\mathrm{vd}}}{U_{\mathrm{dc}}}-\dfrac{1}{2}u_{\mathrm{cpq2}}\dfrac{u_{\mathrm{vd}}}{U_{\mathrm{dc}}} \\ L_{\mathrm{eq}}\dfrac{\mathrm{d}i_{\mathrm{cq}}}{\mathrm{d}t}=U_{\mathrm{tq}}-R_{\mathrm{eq}}i_{\mathrm{cq}}-\omega_2 L_{\mathrm{eq}}i_{\mathrm{cd}}-\dfrac{u_{\mathrm{vq}}}{U_{\mathrm{dc}}}u_{\mathrm{cp0}}+\dfrac{1}{2}u_{\mathrm{cpq}}+\dfrac{1}{2}\dfrac{u_{\mathrm{cird}}}{U_{\mathrm{dc}}}u_{\mathrm{cpq}} \\ \qquad\qquad -\dfrac{1}{2}\dfrac{u_{\mathrm{cirq}}}{U_{\mathrm{dc}}}u_{\mathrm{cpd}}+\dfrac{1}{2}u_{\mathrm{cpd2}}\dfrac{u_{\mathrm{vd}}}{U_{\mathrm{dc}}}-\dfrac{1}{2}u_{\mathrm{cpq2}}\dfrac{u_{\mathrm{vd}}}{U_{\mathrm{dc}}} \end{cases} \tag{A.9}$$

The differential and algebraic equations of the current inner loop control are:

$$\begin{cases} \dfrac{\mathrm{d}x_{\mathrm{ind}}}{\mathrm{d}t}=I_{\mathrm{dref}}-I_{\mathrm{cd}} \\ \dfrac{\mathrm{d}x_{\mathrm{ind}}}{\mathrm{d}t}=I_{\mathrm{qref}}-I_{\mathrm{cq}} \\ u_{\mathrm{vd}}=G_{\mathrm{d}}[u_{\mathrm{td}}+\omega_0 L_{\mathrm{eq}}i_{\mathrm{cq}}-k_{\mathrm{pind}}\left(I_{\mathrm{dref}}-i_{\mathrm{cq}}\right)-k_{\mathrm{iind}}x_{\mathrm{ind}}] \\ u_{\mathrm{vq}}=G_{\mathrm{d}}[u_{\mathrm{tq}}+\omega_0 L_{\mathrm{eq}}i_{\mathrm{cq}}-k_{\mathrm{pind}}\left(I_{\mathrm{qref}}-i_{\mathrm{cq}}\right)-k_{\mathrm{iind}}x_{\mathrm{ind}}] \end{cases}. \tag{A.10}$$

The differential and algebraic equations of the PLL are:

$$\begin{cases} \dfrac{\mathrm{d}x_{\mathrm{utq}}}{\mathrm{d}t}=u_{\mathrm{tq}} \\ \dfrac{\mathrm{d}x_{\mathrm{pll}}}{\mathrm{d}t}=k_{\mathrm{ppll}}u_{\mathrm{tq}}+k_{\mathrm{ipll}}x_{\mathrm{utq}} \\ \omega_2=\omega_0+k_{\mathrm{ppll}}u_{\mathrm{tq}}+k_{\mathrm{ipll}}x_{\mathrm{utq}} \end{cases}. \tag{A.11}$$

The differential and algebraic equations of the CCSC are:

$$\begin{cases} \dfrac{\mathrm{d}x_{\mathrm{cird}}}{\mathrm{d}t}=I_{\mathrm{cirdref}}-I_{\mathrm{cird}} \\ \dfrac{\mathrm{d}x_{\mathrm{cirq}}}{\mathrm{d}t}=I_{\mathrm{cirqref}}-I_{\mathrm{cirq}} \\ u_{\mathrm{cird}}=G_{\mathrm{d}}[k_{\mathrm{pcird}}\left(I_{\mathrm{cirdref}}-i_{\mathrm{cird}}\right)+k_{\mathrm{icird}}x_{\mathrm{cird}}-2\omega_0 L_{\mathrm{a}}i_{\mathrm{cirq}}] \\ u_{\mathrm{cirq}}=G_{\mathrm{d}}[u_{\mathrm{pcirq}}+\left(I_{\mathrm{cirqref}}-i_{\mathrm{cirq}}\right)+k_{\mathrm{icirq}}x_{\mathrm{cirq}}-2\omega_0 L_{\mathrm{a}}i_{\mathrm{cird}}] \end{cases}, \tag{A.12}$$

where $I_{\mathrm{cirdref}}=0$, $I_{\mathrm{cirqref}}=0$.

The algebraic equations of the PCC point voltage are:

$$\begin{cases} u_{\mathrm{sd}}-u_{\mathrm{td}}=i_{\mathrm{cd}}R_{\mathrm{s}}+i_{\mathrm{cq}}\omega_2 L_{\mathrm{s}} \\ u_{\mathrm{sq}}-u_{\mathrm{tq}}=i_{\mathrm{cq}}R_{\mathrm{s}}+i_{\mathrm{cd}}\omega_2 L_{\mathrm{s}} \end{cases}. \tag{A.13}$$

Appendix B

Table B.1. The model parameters of MMC-HVDC system

Parameters	Values
AC system base capacity S_B (MVA)	400
Inductance of the AC system L_s (mH)	98
Resistance of the AC system R_s (Ω)	1.54
Rated capacity of transformer S_{TN} (MVA)	480
Rated ratio of transformer T (kV/kV)	525/200
Leakage reactance of transformer X_T (p.u.)	15%
Inductance of phase reactor L_f (mH)	48
Resistance of phase reactor R_f (Ω)	1.5
Sub module capacitance C (μF)	2 200
Bridge arm inductance L_a (mH)	60
Number of bridge arm sub modules n	40
DC side rated voltage U_{dc} (kV)	±200
Rated power of DC line transmission P_{dc} (MW)	400

Table B.2. The control parameters of MMC-HVDC system

Controllers	Parameters
d-axis outer loop control	$k_{poutd} = 0.01$, $k_{ioutd} = 32$
q-axis outer loop control	$k_{poutq} = 0.01$, $k_{ioutq} = 32$
d-axis current inner loop control	$k_{pind} = 5$, $k_{iind} = 125$
q-axis current inner loop control	$k_{pinq} = 5$, $k_{iinq} = 125$
d-axis CCSC	$k_{pcird} = 0.2$, $k_{icird} = 10$
q-axis CCSC	$k_{pcirq} = 0.2$, $k_{icirq} = 10$
PLL	$k_{ppll} = 50$, $k_{ipll} = 100$

References

[1] Jin H., Luo Y., Fan Y., Pan S., *Improved carrier phase shift modulation and voltage equalization control strategy in modular multilevel converter*, Archives of Electrical Engineering, vol. 68, no. 4, pp. 803–815 (2019), DOI: 10.24425/aee.2019.130684.

[2] Christoph B., Christian R., Andreas M., Jochen J., *BorWin1 – First experiences with harmonic interactions in converter dominated grids*, International ETG Congress 2015, Die Energiewende-Blueprints for the new energy age, Bonn, Germany, pp. 1–7 (2015).

[3] Saad H., Fillion Y., Deschanvres S., Vernay Y., Dennetière S., *On Resonances and Harmonics in HVDC-MMC Station Connected to AC Grid*, IEEE Transactions on Power Delivery, vol. 32, no. 3, pp. 1565–1573 (2017), DOI: 10.1109/TPWRD.2017.2648887.

[4] Zou C., Rao H., Xu S., Li Y., Li W., Chen J., Zhao X., *Analysis of Resonance Between a VSC-HVDC Converter and the AC Grid*, IEEE Transactions on Power Electronics, vol. 33, no. 12, pp. 10157–10168 (2018), DOI: 10.1109/TPEL.2018.2809705.

[5] Li Y., An T., Zhang D., Pei X., Ji K., Tang G., *Analysis and Suppression Control of High Frequency Resonance for MMC-HVDC System*, IEEE Transactions on Power Delivery, vol. 36, no. 6, pp. 3867–3881 (2021), DOI: 10.1109/TPWRD.2021.3049973.

[6] Li G., Ye H., Bin Z., *High-frequency oscillation mechanism analysis of wind farm-side MMC station considering converter transformer stray capacitance*, International Journal of Electrical Power & Energy Systems, vol. 153 (2023), DOI: 10.1016/j.ijepes.2023.109179.

[7] Tang J., Du X., Du C., Tong C., *Research on the Suppression Strategies of High-frequency Oscillation for MMC-HVDC*, 2021 IEEE 1st International Power Electronics and Application Symposium (PEAS), Shanghai, China, pp. 1–5 (2021), DOI: 10.1109/PEAS53589.2021.9628572.

[8] Yang S., Liu K., Qin L., Zhou T., Zhu S., Hong C., *Research Progress of High frequency Oscillation in MMC-HVDC*, vol. 47, no. 10, pp. 3485–3496 (2021), DOI: 10.13336/j.1003-6520.hve.20210940.

[9] Guo X., Liu Z., Li Y., Lu Y., *Characteristic Analysis of High-frequency Resonance of Flexible High Voltage Direct Current and Research on Its Damping Control Strategy*, Proceedings of the CSEE, vol. 40, no. 1, pp. 19–29+370 (2020).

[10] Feng J., Zou C., Yang S., Zhao X., Fu C., *Impedance Modeling and Characteristic Analysis of flexible HVDC System for Medium and high frequency resonance*, Proceedings of the CSEE, vol. 40, no. 15, pp. 4805–4820 (2020).

[11] Mohammad A., Marta M., *Small-Signal Stability Assessment of Power Electronics Based Power Systems: A Discussion of Impedance- and Eigenvalue-Based Methods*, IEEE Transactions on Industry Applications, vol. 53, no. 5, pp. 5014–5030 (2017), DOI: 10.1109/TIA.2017.2712692.

[12] Guo C., Peng Y., Xu L., Yang S., Hu Y., *Analysis on High-frequency Oscillation Mechanism for MMC-HVDC System Considering Influence of Time Delay*, Automation of Electric Power Systems Press, vol. 44, no. 22, pp. 119–126 (2020), DOI: 10.7500/AEPS20200509006.

[13] Li Y., He Z., Pang H., Yang X., Ji K., Huang W., *High Frequency Stability Analysis and Suppression Strategy of MMC-HVDC Systems (Part I): Stability Analysis*, Proceedings of the CSEE, vol. 41, no. 17, pp. 5842–5855 (2021).

[14] Wang F., Liu K., Zhu S., *High-Frequency Resonance Analysis and Stabilization Control Strategy of MMC Based on Eigenvalue Method*, IEEE Access, vol. 9, pp. 16305–16315 (2021), DOI: 10.1109/ACCESS.2021.3052991.

[15] Dong C., Jia H., Jiang Y., *Time-delay Stability Criteria for Power System with Integral Quadratic Form*, Automation of Electric Power Systems, vol. 39, no. 24, pp. 35–40 (2015), DOI: 10.7500/AEPS20150202015.

[16] Zhu J., Hu J., Lin L., Wang Y., Wei C., *High-Frequency Oscillation Mechanism Analysis and Suppression Method of VSC-HVDC*, IEEE Transactions on Power Electronics, vol. 35, no. 9, pp. 8892–8896 (2020), DOI: 10.1109/TPEL.2020.2975092.

[17] Li C., Liu Y., Li Y., He P., Fang Y., Sheng T., *An approach to suppress low-frequency oscillation in the hybrid multi-Infeed HVDC of mixed H_2/H_∞ robust-based control theory*, Archives of Electrical Engineering, vol. 71, no. 1, pp. 109–124 (2022), DOI: 10.24425/aee.2022.140200.

[18] Zhang F., Yao W., Zhang Z., *High-frequency oscillation analysis and suppression strategy of MMC-HVDC system based on generalized eigenvalue*, Electric Power Automation Equipment, vol. 42, no. 8, pp. 174–183 (2022).

[19] Smith O.J.M., *Closer Control of Loops with Dead Time*, Chemical Engineering Progress, vol. 53, no. 5, pp. 217–219 (1957).

[20] Teng N., Zhang J., *Vacuum induction heating furnace temperature control system based on smith fuzzy-PID*, 2014 International Conference on Mechatronics and Control (ICMC), Jinzhou, China, pp. 2207–2210 (2014), DOI: 10.1109/ICMC.2014.7231961.

[21] Kumar S., *Modified smith predictor design for networked control system with time delay*, 2015 International Conference on Energy, Power and Environment: Towards Sustainable Growth (ICEPE), Shillong, India, pp. 1–5 (2015), DOI: 10.1109/EPETSG.2015.7510085.

[22] Luo Y., Xue W., He W., Nie K., Mao Y., Guerrero J.M., *Delay-Compound-Compensation Control for Photoelectric Tracking System Based on Improved Smith Predictor Scheme*, IEEE Photonics Journal, vol. 14, no. 3, pp. 1–8 (2022), DOI: 10.1109/JPHOT.2022.3164202.

[23] Zhang H., Liao X., Li X., Yu J., *LMI-based approach for stability analysis of fuzzy large-scale system with time delays*, 2004 International Conference on Communications, Circuits and Systems (IEEE Cat. No.04EX914), Chengdu, China, pp. 1401–1405 (2004), DOI: 10.1109/ICCCAS.2004.1346437.

[24] Jia H., *Stability of Power System with Time Delays*, Bei Jing: Science Press (2016).

[25] Zhang X., Xia D., Fu Z., Wang G., Xu D., *An Improved Feedforward Control Method Considering PLL Dynamics to Improve Weak Grid Stability of Grid-Connected Inverters*, IEEE Transactions on Industry Applications, vol. 54, no. 5, pp. 5143–5151 (2018), DOI: 10.1109/TIA.2018.2811718.